Promotion of osteochondral repair through immune microenvironment regulation and activation of endogenous chondrogenesis via the release of apoptotic vesicles from donor MSCs

Guangzhao Tian [a,b,1], Han Yin [b,c,1], Jinxuan Zheng [d,1], Rongcheng Yu [d,1], Zhengang Ding [b], Zineng Yan [b], Yiqi Tang [d], Jiang Wu [b], Chao Ning [b], Xun Yuan [b], Chenxi Liao [d], Xiang Sui [b], Zhe Zhao [b], Shuyun Liu [b,**], Weimin Guo [e,***], Quanyi Guo [a,b,*]

[a] School of Medicine, Nankai University, Tianjin, 300071, China
[b] Institute of Orthopedies, Department of Orthopedics, The Fourth Medical Center of PLA General Hospital, National Clinical Research Center for Orthopedics, Sports Medicine & Rehabilitation, 51 Fucheng Road, Haidian District, Beijing, 100142, China
[c] Department of Orthopaedics, Union Hospital, Tongji Medical College, Huazhong University of Science and Technology, Wuhan, 430022, China
[d] Hospital of Stomatology, Guangdong Provincial Key Laboratory of Stomatology, Sun Yat-sen University, Guangzhou, 510055, China
[e] Department of Orthopaedic Surgery, Guangdong Provincial Key Laboratory of Orthopedics and Traumatology, First Affiliated Hospital Sun Yat-Sen University, Guangzhou, 510080, China

ARTICLE INFO

ABSTRACT

Utilizing transplanted human umbilical cord mesenchymal stem cells (HUMSCs) for cartilage defects yielded advanced tissue regeneration, but the underlying mechanism remain elucidated. Early after HUMSCs delivery to the defects, we observed substantial apoptosis. The released apoptotic vesicles (apoVs) of HUMSCs promoted cartilage regeneration by alleviating the chondro-immune microenvironment. ApoVs triggered M2 polarization in macrophages while simultaneously facilitating the chondrogenic differentiation of endogenous MSCs. Mechanistically, in macrophages, miR-100-5p delivered by apoVs activated the MAPK/ERK signaling pathway to promote M2 polarization. In MSCs, let-7i-5p delivered by apoVs promoted chondrogenic differentiation by targeting the eEF2K/p38 MAPK axis. Consequently, a cell-free cartilage regeneration strategy using apoVs combined with a decellularized cartilage extracellular matrix (DCM) scaffold effectively promoted the regeneration of osteochondral defects. Overall, new mechanisms of cartilage regeneration by transplanted MSCs were unconcealed in this study. Moreover, we provided a novel experimental basis for cell-free tissue engineering-based cartilage regeneration utilizing apoVs.

1. Introduction

In recent years, mesenchymal stem cells (MSCs) transplantation has been widely considered a potential treatment strategy for diseases such as diabetes, autoimmune diseases, cartilage injuries, and osteoarthritis (OA) [1–4]. The potential therapeutic mechanisms of this treatment include immune modulation [5], differentiation [6], paracrine signaling [7], and extracellular vesicle (EV) secretion [8]. Previous studies have shown that only a small fraction of transplanted MSCs can survive and integrate into the host [9,10]. A growing body of evidence suggests that transplanted MSCs survive for only a short time in the recipient [11], including after implantation into the root canal [12] and intravenous injection for graft-versus-host disease (GvHD) [13]. Our previous preclinical studies have also indicated that transplanted HUMSCs in scaffolds are minimally present in regenerating cartilage tissue [14,15]. However, in the field of cartilage tissue regeneration, the destiny of

---

transplanted HUMSCs in scaffolds has not been fully elucidated. Whether the non-survival HUMSCs affect cartilage regeneration or not needs more scientific research.

In the human body, billions of cells undergo apoptosis, which is a fundamental metabolic process for maintaining physiological homeostasis, every day [16–18]. During apoptosis, apoptotic vesicles (apoVs), initially referred to as apoptotic bodies (apoBDs), are formed through membrane budding. These vesicles are not merely fragments; they display a specific distribution of intracellular contents and serve as regulators of biological processes [19]. ApoVs, as a subset of EVs, contain various biomolecules, including microRNAs (miRNAs), mRNAs, DNA, lipids, and proteins [17,18,20]. Recently, studies have shown that apoVs play important roles in regulating immune responses and tissue recovery in multiple tissues and organs [21–23]. Nevertheless, the mechanisms by which apoVs affect macrophage polarization and cartilage regeneration have not yet been fully elucidated.

The delicate balance between stem cell-mediated proliferation and apoptosis of adjacent stem cells or somatic cells plays an essential role in tissue regeneration following injury [24]. Studies have shown that apoptotic cell-induced Wnt3 and c-Jun N-terminal kinase (JNK) signaling contributes to compensatory proliferation [25,26]. Recent research has also shown that apoptotic epithelial stem cells promote the proliferation of neighboring stem cells through the cysteine-dependent generation of apoVs containing Wnt8a [27]. Li et al. reported that osteoclast-derived apoVs promoted the osteogenic differentiation of bone marrow MSCs (BMSCs) [23]. This finding suggests that the

plasticity of stem cells enables them to adapt to tissue homeostasis and regenerative needs upon sensing apoptotic cell signaling. However, the impact and mechanisms of apoVs on host MSCs in cartilage regeneration remain unclear. Analyzing the key molecules and pathways involved in how apoptotic vesicles promote cartilage regeneration is crucial for understanding new mechanisms of stem cell-induced regeneration and developing targeted therapeutic strategies for these key molecules and pathways.

In this study, we demonstrated most of donor HUMSCs in DCM scaffolds implanted in cartilage defects underwent apoptosis and then secreted apoVs. ApoVs derived from HUMSCs combined with DCM scaffolds enhanced cartilage regeneration by delivering enriched miR-100-5p and let-7i-5p to the defects. MiR-100-5p, which activated ERK/MAPK pathway, and let-7i-5p, which directly targeted eEF2K/p38 MAPK signaling pathway, orchestrated cartilage defects repair via promoting macrophage M2 polarization and chondrogenesis (see Scheme 1).

2. Materials and methods

2.1. Ethical approval statement

This study was conducted in full compliance with the ethical principles outlined by the Ethics Committee of the Chinese PLA General Hospital.
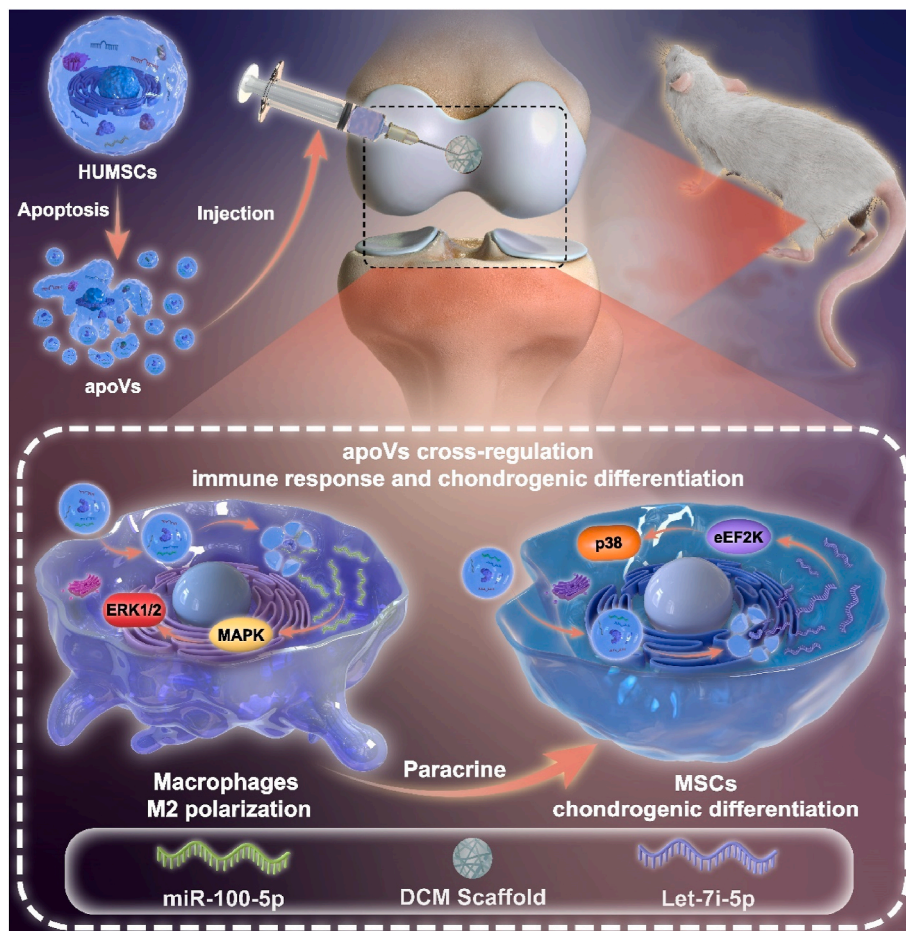
Scheme 1. Schematic summary of our main findings. Intra-articular injection of HUMSC-derived apoVs delivers miR-100-5p into macrophages and promotes M2 macrophage polarization by activating MAPK/ERK1/2, delivers let-7i-5p to MSCs and promotes chondrogenesis by targeting the eEF2K/p38 axis. ApoVs combined with DCM scaffolds facilitate cartilage defect repair. HUMSCs: human umbilical cord-derived mesenchymal stem cells, DCM: decellularized cartilage extracellular matrix.

2.2. Cell culture, apoV collection, and apoV identification

2.2.1. Cell culture

HUMSCs were isolated and extracted per our previous protocol [28] and were cultured with alpha-minimum essential medium (α-MEM) (Corning, USA) supplemented with 10 % fetal bovine serum (FBS) (Gibco, USA) and 1 % penicillin/streptomycin (Invitrogen, USA). Cells at passages 3 to 5 were utilized to ensure viability. The isolation and culture of murine bone marrow-derived macrophages (BMDMs) and BMSCs were performed as previously described [29]. Briefly, male C57BL/6 mice aged 6–8 weeks were purchased from Beijing Weitonglihua Company. The bone marrow was flushed out and then cultured for a period of 7 days in DMEM/F12, 10 % FBS, 50 ng/ml mouse macrophage colony-stimulating factor (M-CSF, PeproTech, USA), 100 U/ml penicillin, and 100 U/ml streptomycin. Forty-eight-hour-old C57BL/6 mice were used for BMSCs isolation. The bone marrow was flushed out and then cultured at 37 °C and 5 % CO_2 in complete culture medium for MSCs: α-MEM, 10 % FBS, 100 μg/ml streptomycin, and 100 U/ml penicillin. BMSCs at passages 3 to 5 were used for subsequent assays.

2.2.2. Induction and characterization of HUMSCs apoptosis

Undifferentiated HUMSCs were rinsed twice with PBS, and the culture medium was replaced with complete medium containing EV-depleted FBS and 250 nM staurosporine (STS) (Cell Signaling Technology, USA). After 3 h of treatment, HUMSCs apoptosis was assessed through morphological observation and TUNEL staining performed with the One Step TUNEL Apoptosis Assay Kit (Beyotime Biotechnology, China) per the manufacturer's protocol.

2.2.3. Isolation and characterization of HUMSC-derived apoVs

ApoVs derived from HUMSCs were obtained with an optimized protocol [21]. Initially, the supernatant of apoptotic cells was harvested 12 h after apoptosis induction and centrifuged at $800 \times g$ for 10 min. The resulting supernatant was further centrifuged at $12,000 \times g$ for 30 min to isolate apoVs, which were then washed twice with filtered PBS. The apoVs were quantified by determining the protein concentration using a BCA Protein Assay Kit (Beyotime Biotechnology, China). ApoVs were characterized with transmission electron microscopy (TEM) (JEOL, Japan) and dynamic light scattering (DLS) (Beckman Coulter, Germany) to assess the morphology and size distribution, respectively. Additionally, Western blotting analysis (details provided in the supplementary materials) was performed to assess specific apoV markers (histone H3, histone H2B, C3b, and C1QC), while Annexin V Fluos labeling reagent staining (Beyotime Biotechnology, China) was utilized for further characterization. Component analysis of apoVs was conducted through proteomic analysis and RNA sequencing (RNA-seq) analysis (details are provided in the supplementary materials).

2.2.4. In vitro internalization of apoVs by BMDMs and BMSCs

DiO-labeled apoVs were coincubated with either BMDMs or BMSCs for various durations (3, 6, 12, and 24 h). Subsequently, the labeled cells were washed thoroughly with fresh culture medium to eliminate any unbound apoVs then fixed with a 4 % paraformaldehyde solution, and stained with DAPI (10 μg/ml). Fluorescence images were acquired using a fluorescence confocal microscope (Nikon, TCS-SP8).

2.2.5. Analysis of apoVs-induced macrophage polarization in vitro

The macrophages were cultured for 24 h and then seeded in well plates at a concentration of 1×10^6 cells/cm². The cells were subsequently incubated in complete macrophage culture medium containing varying concentrations of apoVs (2.5 μg/ml, 5 μg/ml, and 10 μg/ml) for an additional 24 h, with macrophages without added apoVs serving as the control group. Macrophage phenotypes were assessed through immunofluorescence staining (details are provided in the supplementary materials), while specific genes associated with immunomodulation

were analyzed using quantitative real-time polymerase chain reaction (qRT−PCR) (details are provided in the supplementary materials). All primer sequences are listed in Table S1. Additionally, RNA-seq analysis (details provided in the supplementary materials) was conducted to further elucidate the molecular mechanisms involved.

2.2.6. Collection of apoVs-treated BMDMs-conditioned medium (M_{apoVs}-CM)

The native macrophages were exposed to medium containing apoVs at a concentration of 2.5 μg/ml. After two washes with PBS, the cells were cultured in serum-free medium for 24 h. Subsequently, the cell supernatant was collected to obtain M_{apoVs}-CM (apoV-treated macrophage-derived conditioned medium).

2.2.7. Analysis of BMSCs proliferation

Cell proliferation was assessed using a Cell Counting Kit (CCK-8) assay (Dojindo, Japan). BMSCs were seeded in 96-well plates at a density of 2×10^3 cells per well (n = 4) and then incubated in medium containing different concentrations of apoVs (250 ng/ml, 2.5 μg/ml, and 5 μg/ml). Cells cultured in medium without apoVs served as the control group. Additionally, we investigated the impact of M_{apoVs}-CM on BMSCs proliferation by CCK-8.

2.2.8. Scratch assay

BMSCs (5×10^5 cells) were plated in each well of six-well plates at a confluence of 100 %. A scratch was created perpendicular to the horizontal axis using a 10 μl pipette tip. The cells were then treated with either apoVs (250 ng/ml, 2.5 μg/ml and 5 μg/ml) or M_{apoVs}-CM (n = 3). The samples were imaged at 0 h and 12 h using a phase-contrast microscope. The change in the scratch area was quantified using ImageJ software (NIH Image, US).

2.2.9. Transwell assay

Transwell migration assays were conducted as follows: a BMSCs suspension (100 μl; 2×10^5 cells/ml) was added to the upper Transwell compartment (Corning, US). Subsequently, 650 μl of medium was added to the lower chamber, with varying concentrations of apoVs (250 ng/ml, 2.5 μg/ml and 5 μg/ml) or M_{apoVs}-CM. The cells were then cultured at 37 °C for 24 h. Afterward, the migrated cells were stained with DAPI and quantified using ImageJ software.

2.2.10. The effect of apoVs and M_{apoVs}-CM on BMSCs chondrogenic differentiation

To assess the impact of apoVs and M_{apoVs}-CM on BMSC chondrogenic differentiation, we employed pellet aggregate culture as previously described [29]. After a 14-day coculture period in three distinct types of media (standard chondrogenic differentiation medium, M_{apoV}-CM chondrogenic differentiation medium, and apoV chondrogenic differentiation medium), qRT−PCR analysis was conducted to examine the expression levels of chondrogenic genes [ACAN, SOX9, and collagen II (COL2)]. Detailed primer information can be found in Table S1 of the supplementary materials. Subsequently, Safranin O staining, Alcian blue staining, and COL2 immunohistochemistry were carried out on the BMSC pellets after 21 days of chondrogenic differentiation culture.

2.2.11. Transfection of miRNA mimics or inhibitors

MiRNA mimics and inhibitors were procured from RiboBio (Guangzhou, China). BMDMs were differentiated into mature macrophages and subsequently transfected with 50 nM mimics or 100 nM inhibitors of hsa-miR-143-3p, hsa-miR-21-5p, hsa-miR-100-5p, hsa-miR-26a-5p or negative control (RiboBio, China) using Lipofectamine RNAiMAX transfection reagent (Life Technologies, USA). After 24 h, RNA was extracted for qRT−PCR, and the cells were incubated in glass bottom dishes and fixed for fluorescence observation to verify the transfection efficiency. The cells were fixed for immunofluorescence staining and protein extraction after 48 h for Western blot. After 3–5

passages, BMSCs were incubated in 6- or 12-well plates and subjected to transfection with mimics, a negative control mimic, an inhibitor, or an inhibitor negative control of hsa-let-7i-5p using a riboFECT™ CP Transfection kit (RiboBio, China) when they reached 50 % confluence. Transfection efficiency was evaluated by qRT-PCR and fluorescence observation after 24 h. Transfections were performed twice with an interval of 3 days. Chondrogenic differentiation of BMSCs was induced using a Chondrogenic Differentiation Kit (Cyagen, China) according to the instructions at the beginning of miRNA transfection. The chondrogenic media were changed every other day. The cells were harvested for Western blot analysis on the 7th day and for immunofluorescence staining after 21 days (see supplementary materials for details).

2.2.12. Dual-luciferase reporter assay

HEK293T cells were transfected with Firefly/Renilla dual-luciferase vectors (Aidisheng, China) containing wild-type eFF2K-3′UTR (eFF2K-3′UTR-WT) and mutant eFF2K-3′UTR (eFF2K-3′UTR-MU), respectively. Cells seeded in 24-wells plates were co-transfected with let-7i-5p mimic or NC mimic using Lipofectamine 2000 reagent (Invitrogen, USA). Cells were harvested after 24 h, and the luciferase activity was determined by a Luc-pair duo-luciferase assay kit (Beyotime Biotechnology, China). And the level of luciferase activity was calculated as the normalized relative Firefly luciferase/Renilla ratio.

2.2.13. Preparation of DCM scaffolds

The porcine cartilage extracellular matrix and scaffolds were prepared as previous method [36]. Briefly, cartilage pieces were minced. Acetic acid, deionized H_2O, nucleases, PBS, and differential centrifugation were used to decellularize the cartilage tissue. DCM scaffolds were fabricated using a simple freeze-drying and crosslinking method. Scaffolds with a diameter of 2 mm and a thickness of approximately 1 mm were produced and finally sterilized by 60Co γ-irradiation at 5 mRad.

2.2.14. Determination of the HUMSCs fate in cartilage defects

The porcine DCM scaffolds were prepared following previously established methods [30] (see supplementary materials for details). DCM scaffolds loaded with DiO-labeled HUMSCs were implanted into a rat osteochondral defect model. After 0, 1, and 3 days, the scaffolds were fixed, rinsed, and incubated overnight at 4 °C with a primary antibody against Annexin V (1:100; Abcam). After rinsing, the scaffolds were incubated with a fluorescent secondary antibody at room temperature for 1 h. The results were observed under a laser scanning confocal microscope (Nikon, TCS-SP8). Semiquantitative analysis of the results was performed using ImageJ software.

2.2.15. Internalization of apoVs by MSCs and macrophages in vivo

Immunofluorescence was utilized to trace the localization of the injected apoVs, which were labeled with the DiO Green Fluorescent Cell Linker Kit (Abcam, USA), following the manufacturer's instructions. These prelabeled apoVs were injected into the articular cavity of the osteochondral defect model along with DCM scaffolds. Subsequently, the scaffolds were fixed, rinsed, and incubated overnight at 4 °C with primary antibodies against CD105 (1:100; Abcam, USA) or CD68 (1:100; Abcam, USA). After thorough rinsing, the scaffolds were incubated with fluorescent secondary antibodies at room temperature for 1 h. The results were observed using a laser scanning confocal microscope (Nikon, TCS-SP8).

2.2.16. Regulatory effect of apoVs on the articular cavity microenvironment

Nine Sprague–Dawley (SD) rats were randomly assigned to either the PBS group or the apoV group. Under aseptic conditions, a 2.0-mm-diameter trephine was used to create an osteochondral defect approximately 1 mm deep in the femoral trochlea of the left leg, causing slight bleeding. The patella was then repositioned, and the soft tissue and skin

were sutured. Each rat received an injection of either 20 μl of PBS or an equivalent volume of a 1 μg/ml apoV suspension into the knee joint cavity. These injections were repeated every 3 days. After surgery, the rats were allowed free movement and unrestricted access to food. After 7 days, all rats were euthanized, and the joint synovium was collected. Macrophage polarization was evaluated via immunofluorescence staining for CD206 and CD86. Additionally, specific genes associated with immunomodulation (IL-1, TNF-α, Arg-1, and CD206) were analyzed using qRT–PCR.

2.2.17. In vivo cartilage regeneration studies

Eight-week-old male SD rats were randomly allocated to four groups: (A) the control group, (B) the DCM scaffold group, (C) the apoV group and (D) the apoV + DCM scaffold group (n = 5). For the apoV and apoV + DCM scaffold groups, 20 μl of PBS solution containing apoVs was injected into the joint cavity at a concentration of 1 μg/ml, and the medication was administered at 1, 3, and 7 days after surgery. The rats in the control group received an equal volume of PBS.

After sampling, macroscopic evaluation, mechanical property analysis, and microcomputed tomography (micro-CT) analysis were performed for each group to preliminarily analyze the extent of cartilage repair in the defect area. Macroscopic evaluation involves visual inspection of the joint surface to assess gross changes such as tissue color, texture, and the presence of any abnormalities or defects. This approach can provide initial indications of the extent of cartilage repair and any remaining defects. Mechanical property testing provides important information about the strength, stiffness, and overall integrity of the repaired tissue. Through application of controlled compression mechanical forces to the sample, the response of the tissue can be measured, indicating its functional capacity and how well it is integrated with the surrounding tissue. Micro-CT analysis is a powerful imaging technique that allows nondestructive, three-dimensional visualization of bone structure at high resolution. This method can provide quantitative data on parameters such as bone density, volume, and morphology, allowing a detailed assessment of subchondral bone.

Histological examination of cartilage sections at both 6- and 12-weeks post-treatment involved staining with H&E to visualize tissue morphology. For determination of the proteoglycan content and for bone analysis, Safranin O/Fast Green staining was used. The evaluation of histological sections was conducted using the modified O'Driscoll histology scoring system (MODHS), which is tailored for rat cartilage repair, with a sample size of n = 5 for each time point. Additionally, histochemical staining for COL2 (1:200) was carried out to examine the presence of COL2, an essential component of the cartilage matrix. The stained sections were analyzed for COL2 expression levels. Quantitative analysis of COL2 immunohistochemical staining was performed using ImageJ software. This analysis involved assessing three sections from three biological replicates to ensure the robustness and reliability of the results. For comprehensive experimental protocols and methodologies, please consult the Supplementary Information provided.

2.2.18. Statistical analysis

The statistical analysis was conducted using GraphPad Prism 8.0 software, with a significance threshold set at $p < 0.05$. The data are presented as the means ± standard deviations (SD). For comparison of two groups, Student's t tests were used. For comparisons among multiple groups, one-way ANOVA was utilized, followed by a Tukey post hoc test for pairwise comparisons.

3. Results and discussion

3.1. HUMSC apoptosis occurs in transplanted cartilage defects

Stem cell therapy has shown encouraging therapeutic benefits and positive clinical results across a spectrum of diseases and has also proven to be effective for addressing cartilage defects and OA in preclinical

studies and ongoing clinical trials [31–33]. However, the in vivo survival and destiny of transplanted stem cells are still being debated. A recent clinical trial demonstrated the successful regeneration of transparent cartilage in knee joints with cartilage injuries through the transplantation of allogeneic BMSCs without detection of any allogeneic DNA in the newly formed cartilage [34]. This finding suggests that the implanted MSCs may provide initial stimulation but subsequently undergo death and clearance from the tissue. Previous research from our team demonstrated that MSCs loaded into a DCM scaffold effectively increased the repair of cartilage defects [30], but only a few implanted MSCs remained in the repaired tissue [14]. To determine the fate of stem cells implanted in cartilage defects, we implanted DiO-labeled HUMSCs loaded on DCM scaffolds into a rat cartilage defect model. Confocal microscopy revealed a notable reduction in the number of DiO-labeled HUMSCs at 1 and 3 days after implantation, and increased cell apoptosis was demonstrated by an increase in the red fluorescence-labeled specific apoptosis marker Annexin V (Fig. 1A). These findings indicate that many stem cells undergo apoptosis during the early stages after implantation. After transplantation, MSCs undergo cellular death within a brief period of time; this process is primarily attributable to a combination of adverse environmental factors such as nutrient and oxygen deprivation, along with factors such as anoikis—loss of matrix support and adhesion to the ECM—and

inflammation, which precipitates oxidative stress [35,36]. Oxidative stress-induced injury is the primary stimulator of MSC apoptosis [37], while anoikis promotes apoptotic signaling [38], and cellular starvation triggers autophagy [39]. Given the articular microenvironment post-cartilage injury [40] and the types of cell death [41], MSCs introduced into the joint cavity may undergo simultaneous apoptotic, autophagic, and necrotic processes, with apoptosis likely representing the predominant form of death.

Previous studies have shown that systemically injected apoVs are mainly phagocytosed by liver macrophages, which are specialized phagocytic cells involved in clearing apoptotic cells [42,43]. To investigate the distribution and fate of apoVs derived from implanted MSCs in an osteochondral defect model, we first induced the apoptosis of HUMSCs in vivo using STS. The results showed significant changes in cell morphology at 3 h and 12 h and positive TUNEL staining at 3 h (Fig. S1), which confirmed the successful induction of cell apoptosis. We collected apoVs using a gradient centrifugation protocol [44]. The size distribution of apoVs was assessed using DLS analysis. The morphology was evaluated utilizing TEM. As shown in Fig. 1B, apoVs were typically round with a diameter of approximately 1245 nm (Fig. 1C). Immunofluorescence staining demonstrated positive labeling of apoVs with Annexin V (Fig. 1D). Western blot analysis revealed the presence of specific markers, such as histone H3, histone H2B, complement C3b, and
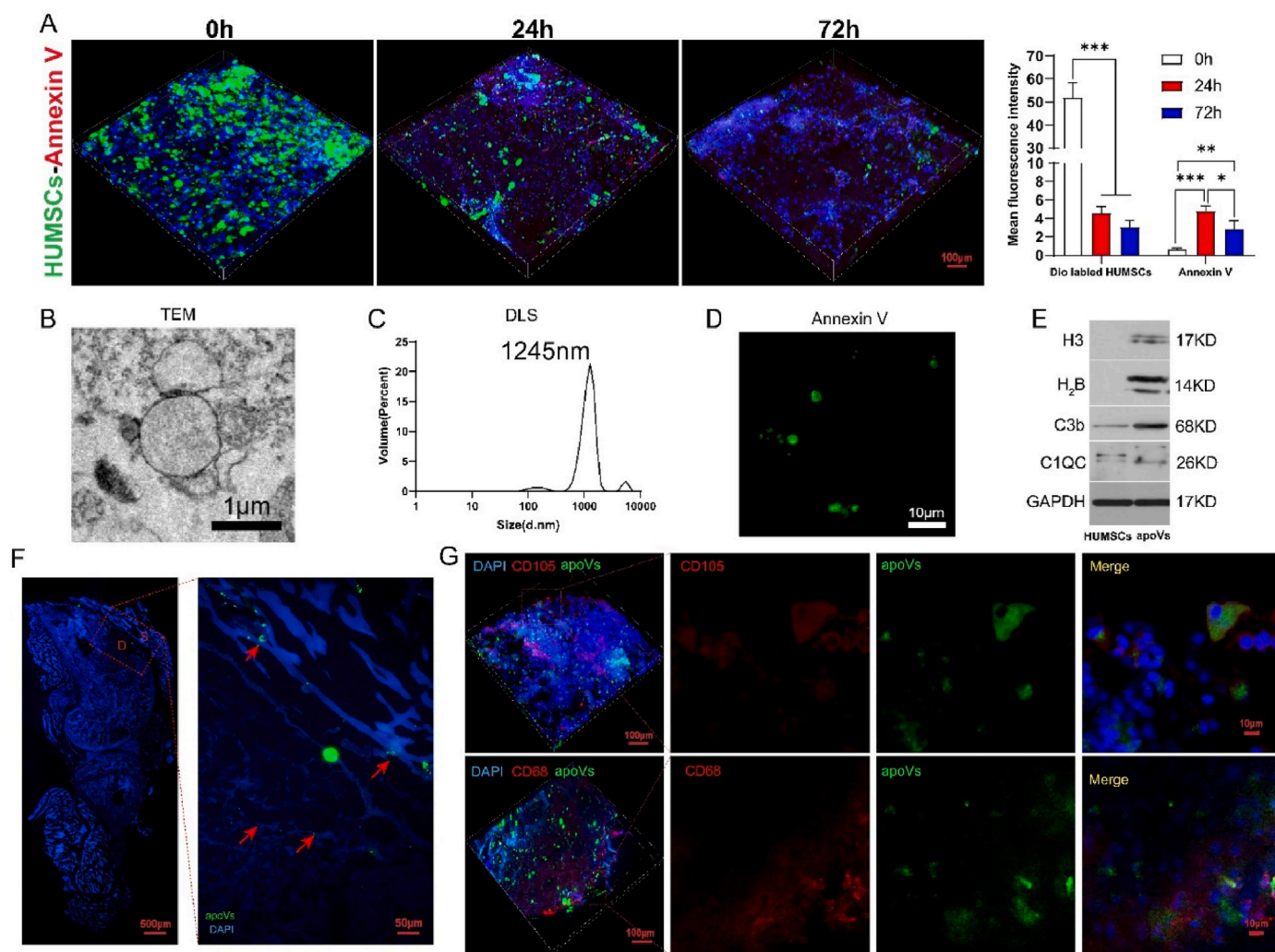
Fig. 1. Fate of transplanted HUMSCs in cartilage defects. (A) Confocal microscopy images illustrating the reduction in HUMSCs and increasing number of apoptotic cells within the DCM scaffold at 0 h, 24 h, and 72 h post-implantation. (B) TEM image showing the morphology of apoVs. (C) Size distribution of apoVs. (D) Confocal microscopy images displaying Annexin V staining of apoVs. (E) Western blot analysis of H3, H2B, C3b, and C1QC in both HUMSCs and apoVs. (F) Distribution of injected apoVs within cartilage defects and the synovium. (G) Phagocytosis of dio-labeled apoVs by MSCs and macrophages within cartilage defects.

complement C1QC (Fig. 1E). Subsequently, DiO-labeled apoVs were administered into the joint cavity of mice with knee articular cartilage defects. Twenty-four hours later, confocal microscopy revealed that green fluorescence was distributed in the defect site and synovium (Fig. 1F). To further explore the internalization of apoVs by cells in vivo, we used a rat model of knee articular cartilage defects and injected DiO-labeled apoVs into the joint cavity. Three days after surgery, immunofluorescence staining was performed to label MSCs with CD105 and macrophages with CD68. As shown in Fig. 1G, both MSCs (red) and macrophages (red) were able to internalize apoVs (green). These results suggest that many MSCs undergo apoptosis shortly after being implanted into the joint cavity and that the apoVs produced are phagocytosed by MSCs and macrophages, which may be a potential mechanism underlying their ability to promote cartilage defect repair and regeneration.

3.2. ApoVs derived from HUMSCs are rich in various functional proteins and miRNAs

Although the scientific community has shown strong interest in EVs originating from viable cells, our current knowledge regarding apoVs generated from apoptotic cells remains limited. The molecular composition of apoVs is a central focus in this area of research due to their payload of diverse functional proteins [45,46]. The packaging of cargo within apoVs depends on the cell type of the parent cell; therefore, apoVs originating from distinct cell types may exhibit varying functionalities [47]. To determine the precise proteomic traits of apoVs derived from HUMSCs, we extracted proteins from both the apoVs and the parent HUMSCs. We then conducted LC−MS/MS analysis, which enabled us to identify a comprehensive sum of 4333 proteins, with 345 upregulated in apoVs (Figs. S2A and B). We performed enrichment and functional analyses of the differentially expressed proteins. In our study, we observed notable upregulation of several crucial apoptotic markers within apoVs, including the apoptosis regulator BAX [48], apoptotic protease activating factor 1 (Apaf-1) [49,50], and p53 apoptosis effector related to PMP-22 (PERP) [51,52]. We utilized the Gene Ontology (GO) database for functional annotation and discovered that the proteins upregulated in apoVs were associated with many terms spanning the three domains "cellular component," "molecular function," and "biological process." This finding suggested that a broad array of functional proteins were encapsulated within apoVs (Fig. S2C). Enrichment analysis revealed that upregulated proteins in apoVs were mainly involved in "cell adhesion," "cell migration," and "integrin-mediated signaling pathway". In terms of cellular components, apoVs were enriched in "extracellular exosome," and in molecular function, they were involved in "calcium ion binding" and "integrin binding." During the biological process enrichment analysis, we additionally identified upregulated proteins within apoVs that played roles in "regulating macrophage migration" and "maintaining stem cell populations" (Fig. S2D). Furthermore, we explored the signaling pathways involving these upregulated proteins through Kyoto Encyclopedia of Genes and Genomes (KEGG) pathway analysis. Our findings illustrated that these proteins play important roles in the "ECM-receptor interaction" and "cell adhesion molecule" signaling pathways (Fig. S2E). The KEGG results further indicated that these proteins are linked to various processes and pathways across different domains. Specifically, in the "cellular process" domain, these proteins are associated with "cellular community," "transport and catabolism," and "cell growth and death." In the "environmental information processing" domain, these proteins are involved in "signal transduction." Additionally, in the "human diseases" domain, the proteins are implicated in "immune disease." In terms of metabolism, these proteins play a role in "carbohydrate metabolism." Moreover, within the "organismal systems" domain, the proteins are associated with the "immune system," "nervous system," and "endocrine system" (Fig. S2F). Protein-protein interaction (PPI) analysis revealed a complex network illustrating the functional interplay among proteins

(Fig. S2G). These results underscore the abundance of functionally relevant proteins within apoVs, particularly those closely tied to cellular behavior, signal transduction, and the modulation of both immunity and metabolism. We identified a notable enrichment of specific proteins in apoVs that play a role in the regulation of macrophage anti-inflammatory (M2) polarization. These proteins include the 60 kDa heat shock protein (HSPD1), which is a small heat shock protein known to effectively promote macrophage M2 polarization [53]; Annexin A5 (ANXA5), which has been shown to play a specific role in the phenotypic polarization of liver macrophages from M1 to M2 [54]; and integrin alpha-5 (ITGA5), which may be an important regulator of tumor immune cell infiltration [55]. These proteins may mediate the immunoregulatory effects of apoVs at the molecular level.

We also performed miRNA sequencing of apoVs to further characterize their molecular composition. The miRNA expression levels were quantified using the transcript per million (TPM) metric [56]. We screened for miRNAs with TPM>2 and identified a total of 343 miRNAs for GO analysis. The relative expression levels of the top 20 miRNAs are shown in Fig. 2A. Using the GO database, we categorized the target genes into various terms from the "biological process," "cellular component," and "molecular function" domains. This analysis delineates the payload of diverse active molecules within apoVs (Fig. 2B). To further explore the involvement of miRNAs in cartilage regeneration and repair, we conducted enrichment analysis on the GO terms associated with target genes using the keywords "stem cell" and "macrophage". The findings revealed that the miRNAs contained in apoVs primarily contribute to "stem cell maintenance and differentiation" (Fig. 2C). Furthermore, pathway enrichment analysis utilizing the KEGG database revealed that genes associated with stem cells are involved in the "Wnt and Hippo signaling pathways" (Fig. 2E). Moreover, the GO analysis of target genes specifically chosen for macrophages illustrated that the miRNAs found in apoVs primarily engage in "macrophage activation, chemotaxis, and differentiation" (Fig. 2D). KEGG analysis revealed that the genes related to macrophages are primarily involved in the "Toll-like receptor signaling pathway" (Fig. 2F). These discoveries have contributed to our understanding of HUMSC-derived apoVs and serve as a reference for our subsequent studies.

3.3. ApoVs facilitate M2 polarization of macrophages by delivering miR-100-5p to activate the MAPK/ERK signaling pathway

Given our observation of macrophages phagocytizing apoVs in vivo, coupled with their crucial involvement in tissue regeneration and homeostasis, we identified a notable connection between macrophages and the uptake of apoVs, underscoring their essential contribution to tissue equilibrium [57]. In particular, M2 macrophages are crucial for regulating inflammation and tissue repair [58–60]. Recent research has shown the important roles of M2 macrophages in OA and chondrogenesis [61–63]. Our aim was to investigate whether internalization of apoVs induces phenotypic changes in macrophages. The isolation and characterization of mouse BMDMs were detailed in our prior investigation [29]. After addition of DiO-labeled apoVs to cultured BMDMs, we observed that apoVs were internalized by BMDMs in a time-dependent manner using confocal microscopy (Fig. 3A). To investigate the effects of apoVs on macrophage phenotype, we first conducted a dose−response analysis of apoVs. Our results indicated a significant increase in the expression of the M2 marker CD206 following treatment with apoVs, while there was no significant increase in the expression of M1 markers after treatment with different concentrations of apoVs (Fig. S3A). We also observed a notable decrease in the expression levels of M1 inflammatory markers such as iNOS, TNF-α, and IL-6. Conversely, we observed a marked increase in the expression of M2 macrophage markers, including CD206, Arginase-1, and TGF-β1 (Fig. S3B). Given its cost-effectiveness, we chose to use 2.5 μg/ml apoVs for subsequent experiments. We further introduced lipopolysaccharide (LPS)-induced M1 macrophages as a positive control to confirm the effects of apoVs on the

Fig. 2. Characterization of apoVs via miRNA sequencing. (A) The top 20 most abundant miRNAs of apoVs. (B) GO analysis of target genes with TPM>2 for miRNAs. (C) GO analysis of target genes associated with stem cells. (D) GO analysis of target genes associated with macrophages. (E) KEGG pathway analysis of the target genes in (C). (F) KEGG pathway analysis of the target genes in (D). SSC: somatic stem cell, HSC: hematopoietic stem cell, MSC: mesenchymal stem cell, NSC: neuronal stem cell, ANS: autonomic nervous system, SNS: sympathetic nervous system, M: macrophages, GM-CSF: granulocyte-macrophage colony-stimulating factor, M-CSF: macrophage colony-stimulating factor, D: differentiation.

macrophage phenotype. LPS-induced macrophages expressed high levels of M1-related markers, while macrophages treated with apoVs expressed high levels of M2-related markers (Fig. 3B–F). These data strongly suggest that the internalization of apoVs promotes M2 polarization of macrophages.

To further elucidate the gene expression profile of BMDMs treated with apoVs, we performed RNA transcriptome profiling analysis of apoV-treated BMDMs and control BMDMs. Our analysis identified 3317 differentially expressed genes (DEGs), comprising 1492 upregulated genes and 1825 downregulated genes (Fig. S4A). Functional analysis utilizing the GO database highlighted the annotation of the 3317

identified DEGs. This finding underscores the extensive transcriptional alterations induced in BMDMs after apoV internalization (Fig. S4B). Notably, within the 'biological process' category, DEGs associated with immunity and inflammation were significantly enriched. These terms included "immune response", "immune system process", "intracellular signal transduction", and "negative regulation of interleukin-6 production" (Fig. 3E). KEGG pathway enrichment analysis indicated a significant enrichment in inflammation-related pathways among the DEGs following apoV internalization. Notably, pathways such as the MAPK, NOD-like receptor, and TNF pathways were highly enriched (Fig. 3F). Among these pathways, the MAPK signaling pathway is associated with
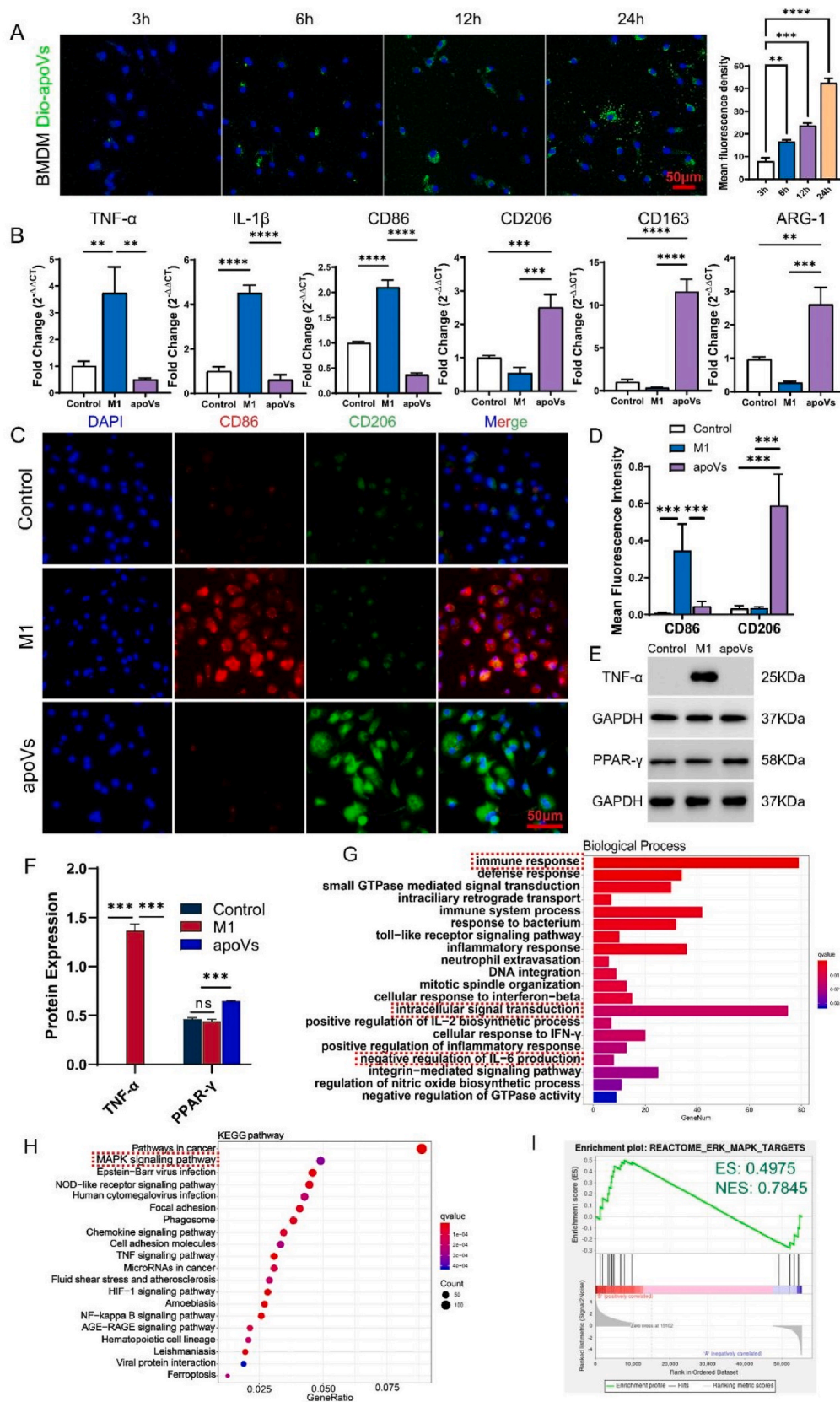
Fig. 3. Efferocytosis of apoVs induced M2 polarization of BMDMs in vitro. (A) Time-dependent engulf of dio-labeled apoVs by BMDMs, with average fluorescence intensity quantified (n = 3). (B) Relative mRNA levels of M1 marker genes (TNF-α, IL-β and CD86) and M2 marker genes (CD206, CD163 and Arginase-1) in BMDMs cultured with apoVs (n = 3). (C) Immunostaining for CD206 and CD86 of BMDMs after incubation with apoVs. (D) Quantitative analysis of fluorescently stained CD86 and CD206 (n = 3). (E) Western blot analysis of TNF-α (M1) and PPAR-γ (M2) expression levels. (F) Quantitative analysis of western blot (n = 3) (G) Biological process enrichment analysis of the differentially expressed genes (DEGs) in BMDMs. (H) KEGG pathway analysis of the DEGs. (I) GSEA revealing a significant increase in MAPK/ERK pathway gene enrichment score in BMDM + apoVs.

M2 polarization of macrophages [64]. Gene set enrichment analysis (GSEA) revealed the upregulation of characteristic genes associated with the MAPK/ERK signaling pathway in BMDMs following apoV treatment (Fig. 3G).

Numerous studies have suggested that EVs mediate cellular communication by delivering miRNAs [65,66]. Based on the miRNA expression profile of HUMSC-apoVs determined by miRNA sequencing (Fig. 2A), to further investigate the molecular mechanism underlying apoV-induced M2 polarization of macrophages, we screened the four most abundant miRNAs in apoVs: let-7i-5p, miR-143-3p, miR-100-5p, and miR-21-5p. Mouse BMDMs were cocultured with mimics or inhibitors of these four miRNAs, a negative control mimic (NC mimic), or a negative control inhibitor (NC inhibitor). The transfection efficacy was confirmed through fluorescence labeling in mimic or inhibitor internalization experiments and qRT−PCR (Fig. S5). Immunofluorescence staining of macrophage polarization markers demonstrated a significant increase in the expression of the M2 marker CD206 and a decrease in the expression of the M1 marker CD86 upon treatment with the miR-100-5p mimic (Fig. 4A). Analysis of macrophage polarization-related gene expression revealed significant changes in various groups. Specifically, the miR-100-5p mimic substantially upregulated the expression of genes such as CD206 and Arginase-1 (M2) while downregulating the expression of genes such as IL-6 and iNOS (M1). In contrast, inhibition of miR-100-5p led to a notable decrease in CD206 and Arginase-1 expression, accompanied by an increase in IL-6 and iNOS expression (Fig. 4B). These findings demonstrate that miR-100-5p is a candidate for M2 polarization of macrophages. Macrophage transcriptome sequencing revealed significant enrichment of the MAPK signaling pathway after apoV treatment (Fig. 3F). The MAPK cascade plays a crucial role as an oncogenic factor in driving M2-like activation of macrophages [64,67, 68]. To explore the potential involvement of miR-100-5p in the activation of the MAPK pathway, we assessed the levels of key pathway-associated proteins, such as ERK1/2, p38, and JNK, using Western blot analysis. As shown in Fig. 4C and D, the miR-100-5p mimic significantly increased the phosphorylation of ERK1/2. Previous studies have reported that phosphorylation of ERK promotes M2 polarization of macrophages [69–71]. Hence, these findings suggest that apoVs facilitate M2 polarization of macrophages through the delivery of miR-100-5p, leading to the activation of the MAPK/ERK signaling pathway.

3.4. ApoVs and ApoVs treated macrophages promote proliferation, migration, and chondrogenic differentiation of MSCs in vitro

The migration of host stem cells to the injury site and their subsequent differentiation into chondrocytes is a crucial process for cartilage repair and regeneration [72]. The paracrine effects of different phenotypes of macrophages regulate stem cell chondrogenic differentiation [29,62]. Hence, we further investigated the impact of apoVs and apoV-treated macrophages on the functionality of MSCs. First, coculture of DiO-labeled apoVs with BMSCs resulted in a time-dependent internalization of apoVs by BMSCs (Fig. 5A). To investigate the functional impact of internalized apoVs on the biological processes of BMSCs, we exposed BMSCs to varying concentrations of apoVs. Interestingly, while apoV treatment did not lead to an increase in the expression of chondrogenic genes (ACAN, COL2, and SOX9), it did increase the expression of critical factors associated with stem cell chondrogenic differentiation, such as TGF-β3 and IGF. Moreover, apoVs notably stimulated the expression of macrophage chemoattractant factor (CCL3) and promoted the expression of genes related to anti-inflammatory cytokines (IL-4 and PGE2) (Fig. S6A). These results suggest that after the internalization of apoVs, BMSCs activate their paracrine functions, potentially positively affecting surrounding stem cells and M2 macrophage polarization, aiding in cartilage repair. We further investigated the biological functions of BMSCs. During proliferation, following a 5-day coculture period, apoV treatment notably increased the proliferation of BMSCs, with the most pronounced effect observed at a concentration of 2.5 μg/ml (Fig. 5B). For migration studies, scratch wound assays demonstrated that the apoV group exhibited faster wound closure than did the control group (Fig. 5C). Transwell assays revealed a greater number of migrating cells in the apoV group than in the control group (Fig. 5D).

During the functional metamorphosis of autologous MSCs, the interplay between different cell types has emerged as pivotal for tissue repair. Given the functional modulation of macrophages, we hypothesized that apoV-treated macrophages might exert additional effects on MSC functionality. To explore this hypothesis further, we procured conditioned medium derived from macrophages subjected to apoV treatment (M_{apoVs}-CM) and further treated BMSCs with conditioned medium. CCK-8 proliferation assays indicated that M_{apoVs}-CM augmented the proliferative capacity of BMSCs (Fig. S6B). Transwell assays indicated that M_{apoVs}-CM reduced the migration of MSCs (Fig. S6C).

The chondrogenic differentiation of endogenous stem cells is a key step in cartilage repair. We investigated the effects of apoVs and M_{apoVs}-CM on the chondrogenic differentiation of BMSCs. We induced chondrogenic differentiation using pellet culture and coincubated BMSCs microspheres with apoVs and M_{apoVs}-CM for 14 or 21 days, followed by qRT−PCR assays and analysis of the mRNA levels of chondrogenic genes, including ACAN, SOX9, and COL2. As shown in Fig. 5E, compared to the control group, the M_{apoVs}-CM group exhibited elevated expression levels of the SOX9 and COL2 genes, while the apoV group exhibited elevated mRNA levels of all three genes. Furthermore, we analyzed the BMSC microspheres using Alcian blue staining. The staining intensity was greater in the M_{apoVs}-CM group than in the control group and even greater in the apoV group. Quantitative analysis revealed that apoVs and M_{apoVs}-CM promoted the secretion of glycosaminoglycans by BMSCs during chondrogenic differentiation (Fig. 5F). We also analyzed frozen sections of 21-day differentiated BMSC microspheres using Safranin O, Alcian blue, and COL2 immunohistochemical staining. As shown in Fig. 5G, compared to those in the control group, apoV and M_{apoVs}-CM significantly promoted the deposition of cartilage ECM-related substances. These results suggest that apoVs and apoV-treated macrophages contribute to the chondrogenic differentiation of BMSCs.

3.5. ApoVs promote the chondrogenic differentiation of BMSCs through the delivery of let-7i-5p targeting the eEF2K/p38 MAPK axis

Next, we investigated the mechanism through which apoVs promote the chondrogenic differentiation of BMSCs. MiRNA sequencing of HUMSC-apoVs revealed that let-7i-5p showed the highest abundance (Fig. 3A). Previous reports have demonstrated the close association of let-7i-5p with the osteogenic differentiation of MSCs [73,74], along with its role in modulating the TGF-β signaling pathway [75]. Therefore, we hypothesized that let-7i-5p might be a key effector molecule responsible for apoV-mediated chondrogenic differentiation of BMSCs. BMSCs were cocultured with mimics or inhibitors of let-7i-5p, NC mimic, or NC inhibitor. The transfection efficacy was confirmed through fluorescence labeling in mimic or inhibitor internalization experiments and qRT−PCR (Fig. S5). We initially verified that let-7i-5p mimics stimulated the expression of chondrogenic proteins, notably ACAN, SOX9, and COL2, in BMSCs (Fig. 6A). To identify the target genes of let-7i-5p in BMSCs, we predicted them via miRDB, TargetScan, and microT-CDS. Notably, bioinformatic analysis predicted that eEF2K is a possible target gene of let-7i-5p. The database analysis revealed that let-7i-5p can bind to the 3′ untranslated region (UTR) of eEF2K (Fig. 6B). To further validate this interaction experimentally, we generated luciferase reporter plasmids containing either the wild-type (WT-pmirGLO-eEF2K) or mutated (MUT-pmirGLO-eEF2K) 3′-UTRs of eEF2K and transfected them into 293T cells. Upon stimulation with let-7i-5p, luciferase activity was attenuated, indicating direct binding between let-7i-5p and eEF2K. This effect was abolished when the 3′-UTR of eEF2K was mutated (Fig. 6C). Eukaryotic elongation factor 2 kinase (eEF2K), belonging to the
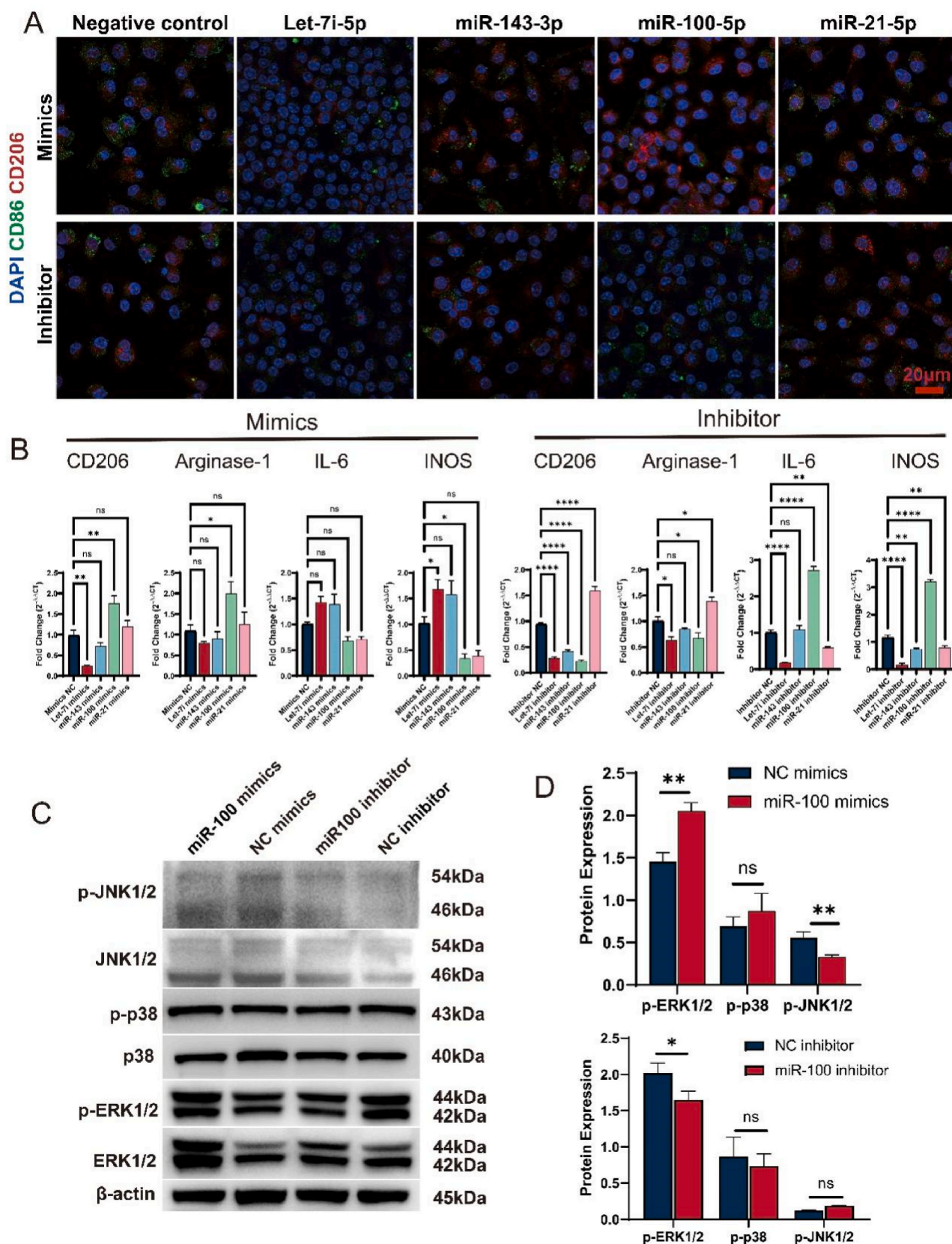
Fig. 4. MiR-100-5p promoted macrophage M2 polarization by activating the MAPK/ERK signaling pathway. (A) Representative immunofluorescence images showing the expression of macrophage markers in BMDMs transfected with different miRNA mimics or inhibitors. (B) Relative mRNA levels of M2 marker genes (CD206 and Arginase-1) and M1 marker genes (IL-6 and iNOS) in BMDMs transfected with different miRNA mimics or inhibitors. (C, D) Western blot analysis of the MAPK pathway in BMDMs.
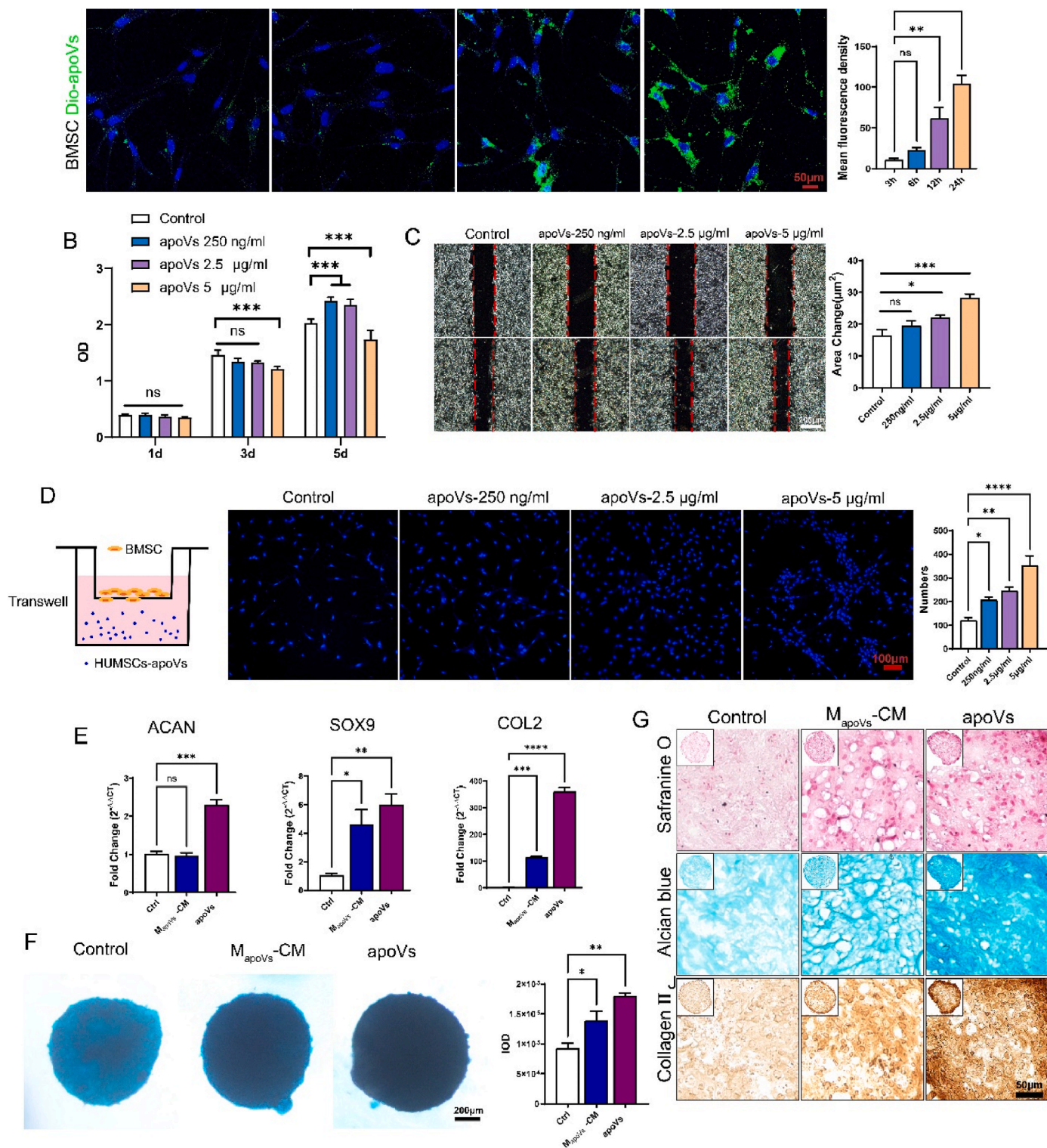
Fig. 5. Effects of apoVs and M$_{apoVs}$-CM on BMSC migration, proliferation and chondrogenesis in vitro. (A) Time-dependent uptake of DiO-labeled apoVs (green) by BMSCs, and the average fluorescence intensity of each cell was quantified (n = 3). (B) CCK-8 assay of BMSC proliferation after culture with different concentrations of apoVs (n = 4). (C) Scratch assay examining the migration of BMSCs cultured with different concentrations of apoVs (n = 4). (D) Transwell assay examining the migration of BMSCs cultured with different concentrations of apoVs (n = 3). (E) Relative mRNA expression levels of chondrogenesis-related genes in BMSCs after induction of chondrogenic differentiation (n = 3). (F) Alcian blue staining of BMSC pellets after induction of chondrogenic differentiation and relative quantification analysis (n = 3). (G) Safranin O and Alcian blue staining and COL2 immunohistochemistry of BMSC pellets after induction of chondrogenic differentiation.

Fig. 6. Let-7i-5p is an effector of apoV-mediated BMSC chondrogenic differentiation by targeting the eEF2K/p38 MAPK axis. (A) Immunofluorescence of ACAN, SOX9, and COL2 in BMSC pellets transfected with let-7i-5p mimics or inhibitors and treated with chondrogenic differentiation medium. (B) Bioinformatic analysis was used to predict the potential target sequences of let-7i-5p. (C) Relative luciferase activity of 3′-UTR-eEF2K-luc constructs in HEK293T cells after transfection of let-7i-5p mimics. (D–F) The protein expr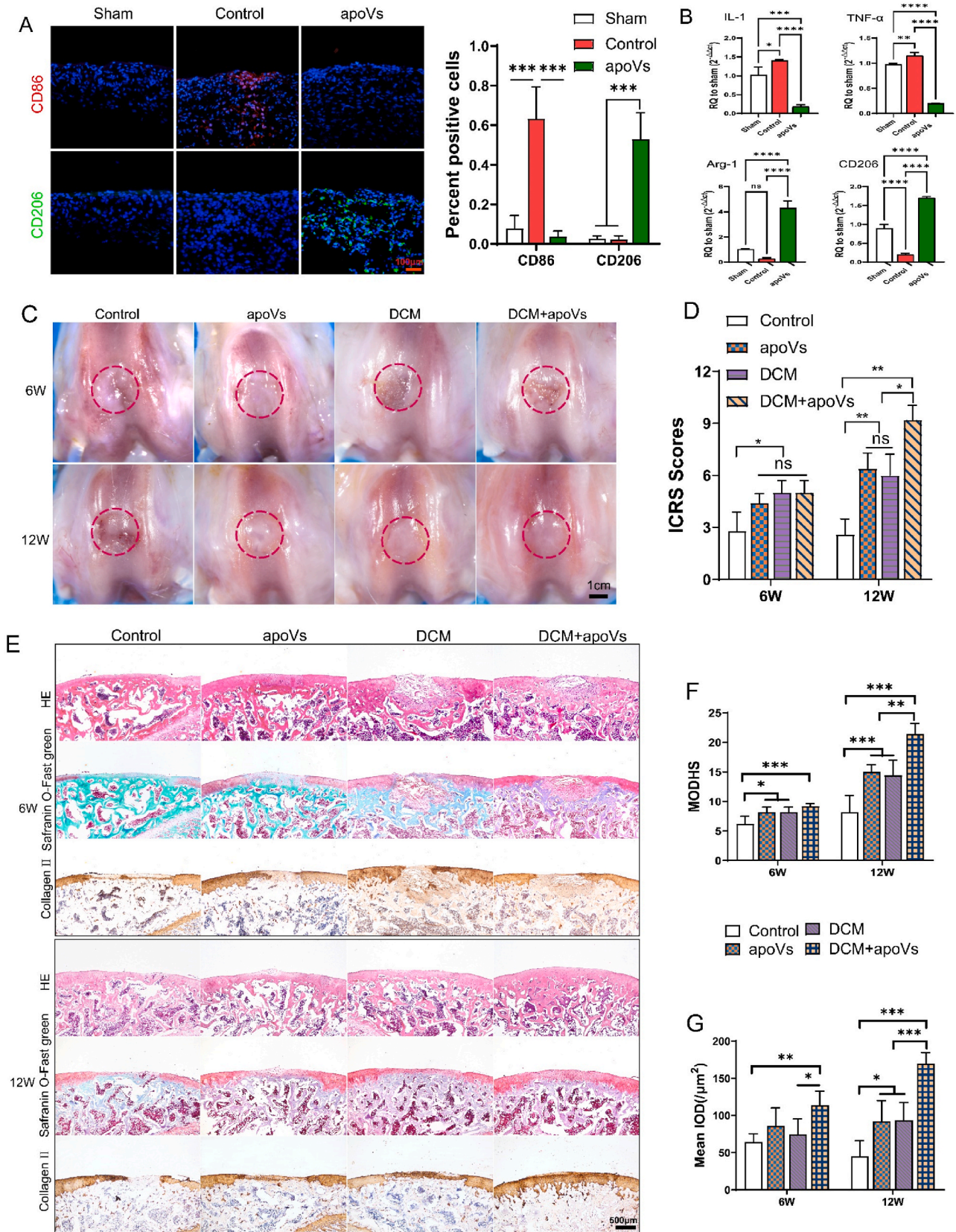ession of BMSCs treated with chondrogenic differentiation medium and transfected with let-7i-5p mimics or inhibitors (n = 3, p < 0.05).

calcium/calmodulin-dependent kinase family, functions as a negative regulator of protein synthesis. Previous research has shown that the inhibition of eEF2K promotes myofibroblast proliferation and differentiation through the p38 MAPK signaling pathway [76]. The activation of the p38/MAPK pathway has been reported to be closely linked with the chondrogenic differentiation of MSCs [77–79]. We explored whether let-7i-5p increases p38 MAPK pathway activation via eEF2K inhibition, thereby promoting chondrogenic differentiation of MSCs. We utilized Western blot analysis to evaluate the expression levels of pertinent proteins in BMSCs following chondrogenic induction in cells transfected with let-7i-5p mimics or inhibitor. Compared to that in the control group, the protein expression of both total eEF2K and phosphorylated eEF2K in the let-7i-5p mimic group decreased (Fig. 6D and E). Moreover, the let-7i-5p mimics substantially increased p38 phosphorylation and upregulated the expression of the chondrogenic markers COL2 and SOX9 (Fig. 6D and E). The let-7i-5p inhibitor decreased the expression of COL2, SOX9 and phosphorylated p38 but significantly increased the expression of eEF2K (Fig. 6D–F). These findings indicate that let-7i-5p decreases both the expression and activation of eEF2K in BMSCs, which in turn promotes p38 MAPK signaling to support chondrogenic differentiation.

3.6. Promotion of M2 polarization of synovial macrophages by ApoVs derived from HUMSCs

Given the in vitro evidence that apoVs promote M2 polarization of

macrophages, we examined the effects of apoVs on synovial macrophages in vivo. First, the retention of DiO-labeled apoVs in the joint cavity was proven through live fluorescence imaging (Fig. S7). At 3 days post-injection, there was only a small amount of fluorescence signal, which completely disappeared after 5 days. Then, immunofluorescence staining and qRT–PCR were conducted on synovial knee joint tissue to assess M2 macrophage polarization. The immunofluorescence results revealed a notable increase in the M2 macrophage marker CD206 and a concurrent decrease in the M1 marker CD86 in the apoV-treated group (Fig. 7A). In the apoV group, the expression levels of the proinflammatory cytokines IL-1 and TNF-α were substantially lower, while the expression levels of the M2 macrophage-associated genes arg-1 and CD206 were significantly greater (Fig. 7B). These results suggest that apoVs promote M2 polarization of macrophages in vivo, modulating the articular immune microenvironment toward an anti-inflammatory and proregenerative state, thus providing favorable conditions for cartilage regeneration and repair.

3.7. HUMSCs-derived apoVs combined with DCM scaffolds promote osteochondral defects repair

OA is a major threat to global health [80]. Cartilage defects are common in the progression of OA and are a major challenge in clinical practice due to the inherent limitations in their self-healing capacity attributed to their low cellularity and avascular nature. Extensive strides have been made in exploring various approaches, such as biomaterials,

Fig. 7. Regulatory effect on the articular microenvironment and evaluation of cartilage regeneration in vivo (A) Immunofluorescence analysis of the M1 and M2 macrophage markers of synovial macrophages and relative quantification of M1 and M2 macrophages (n = 3). (B) qRT-PCR analysis of the mRNA expression levels of IL-1, TNF-α, Arg-1, and CD206 in the synovium (n = 3). (C) Representative microscopic observation of the repaired tissues at 6- and 12-weeks post-surgery. (D) ICRS score for macroscopic assessment. (n = 5). (E) Histological (HE, Safranin O-Fast Green) and immunohistochemical analyses of the osteochondral defect at 6 and 12 weeks. (F) MODHS histological evaluations of repaired cartilage (n = 5). (G) Quantitative analysis of COL2 immunohistochemical staining (n = 5).

MSCs, and their derivatives, aimed at facilitating cartilage repair. These endeavors show promise for resolving this medical conundrum through regenerative strategies [10,81]. Our prior research showed that DCM scaffolds feature a highly interconnected porous structure that effectively promotes the proliferation of MSCs. In addition, DCM scaffolds loaded with different MSCs have achieved satisfactory cartilage repair effects in sheep, rabbit, and rat cartilage defect models [29,82–85]. However, cell therapy under clinical conditions has various limitations, including immunogenicity, uncontrolled cell differentiation, and tumorigenic risks [86,87]. Hence, we proceeded to devise a proof-of-concept investigation to assess the therapeutic efficacy of apoVs in conjunction with DCM scaffolds rather than relying on stem cells alone in a rat model of osteochondral defects. The outcomes of the repair were assessed at 6 and 12 weeks following the surgical procedure. As illustrated in Figs. 7C and 6 weeks after surgery, the control group displayed white fibrous tissue filling the defect site, characterized by a coarse surface texture and distinct demarcation from the surrounding cartilage. The apoV group showed relatively even white fibrous tissue filling. The DCM group and DCM + apoV group displayed partially regenerative transparent cartilaginous tissue. At 12 weeks post-implantation, the DCM + apoV group exhibited obvious repair of the cartilage defect, while the regenerative tissue in the control group was less voluminous than the adjacent healthy cartilage. The apoV group and DCM group exhibited repair tissues of similar heights to the surrounding normal cartilage, indicating successful regeneration. These findings were further corroborated by the international cartilage repair society (ICRS) scores, providing additional validation of the study's outcomes (Fig. 7D–S8).

We assessed the cartilage defect areas of each group using H&E, Safranin O/Fast Green, and COL2 immunohistochemical staining (Fig. 7E). At 6 weeks, no regenerative cartilage tissue was observed in the defect areas of any of the groups. Notably, the subchondral bone displayed evident gaps and cavities, with partial retention of the implanted DCM. However, by the 12-week mark, the defects in the DCM + apoV group were filled with uniformly smooth regenerative tissue. The ECM in the regenerative area exhibited transparent cartilage characteristics, including the production of COL2 and glycosaminoglycans. In contrast, both the apoV group and DCM group displayed a decrease in the thickness of the partially regenerated cartilage, while the control group exhibited no significant generation of transparent cartilage. Consistent with the staining results, the O'Driscoll scores (Fig. 7F) and the relative quantification of COL2 by immunohistochemistry (Fig. 7G) indicated that the DCM + apoV group achieved the highest content of COL2 and histological scores at 12 weeks.

Micro-CT analysis revealed successful subchondral bone repair in the DCM + apoV group, whereas the control group exhibited uneven bone surfaces and bone remodeling, possibly due to persistent inflammatory reactions (Fig. S9A). We conducted further analysis of important indicators of subchondral bone, including bone mineral density (BMD) and bone volume/tissue volume (BV/TV) (Figs. S9B and C). The findings revealed a significant increase in regenerative bone tissue in the DCM + apoV group compared to that in the control group. Additionally, we assessed the Young's modulus of the regenerated tissue, a key functional indicator of articular cartilage, using the nanoindentation technique (Fig. S9D). The results indicated a notably greater Young's modulus in the DCM + apoV group than in the control group at 12 weeks, aligning more closely with the characteristics of normal cartilage tissue. These findings strongly suggest that the combination of DCM and apoVs effectively promotes in vivo regenerative repair of articular cartilage. This study provides novel research evidence supporting the potential of apoVs as therapeutic agents for cartilage defect repair.

4. Conclusion

Our study revealed the initial apoptosis of HUMSCs post-implantation in cartilage defects and highlighted the potential of apoVs derived from MSCs to promote cartilage defect repair. These vesicles regulate macrophage M2 polarization and increase MSC chondrogenic differentiation while also suppressing inflammation and facilitating cartilage regeneration. Mechanistically, miR-100-5p delivered by apoVs activates the MAPK/ERK pathway in macrophages, promoting M2 polarization, while let-7i-5p targets the eEF2K/p38 MAPK axis in MSCs to increase chondrogenic differentiation. The effectiveness of combining apoVs with a DCM scaffold was confirmed in a rat model of osteochondral defects. In summary, our findings broaden the understanding of the role of apoVs in cartilage regeneration, offering promise for treating articular cartilage defects. Furthermore, these insights underscore the potential of using apoVs as an alternative to MSCs for cartilage repair. By elucidating the mechanisms through which apoVs influence cartilage regeneration, our research opens new avenues for developing therapies that could leverage apoVs to enhance tissue repair and regeneration. This advancement offers a novel approach that could overcome some limitations associated with MSC-based treatments and improve clinical outcomes in regenerative medicine. Future research should focus on elucidating the spatiotemporal distribution of apoVs post-injection and optimizing dosimetry for effective cartilage regeneration in both small and large animal models, as well as scaling up apoVs production for clinical translation.

CRediT authorship contribution statement

Guangzhao Tian: Writing – original draft, Methodology, Investigation, Conceptualization. **Han Yin:** Writing – original draft, Methodology, Investigation, Conceptualization. **Jinxuan Zheng:** Writing – original draft, Project administration, Methodology. **Rongcheng Yu:** Project administration, Methodology, Investigation. **Zhengang Ding:** Project administration, Methodology. **Zineng Yan:** Project administration, Methodology. **Yiqi Tang:** Project administration, Methodology. **Jiang Wu:** Project administration, Methodology. **Chao Ning:** Project administration, Methodology. **Xun Yuan:** Methodology. **Chenxi Liao:** Data curation, Methodology. **Xiang Sui:** Methodology. **Zhe Zhao:** Project administration. **Shuyun Liu:** Writing – review & editing, Supervision, Project administration, Methodology, Conceptualization. **Weimin Guo:** Writing – review & editing, Supervision, Project administration, Conceptualization. **Quanyi Guo:** Writing – review & editing, Supervision, Funding acquisition, Conceptualization.

Declaration of competing interest

The authors declare that they have no known competing financial interests or personal relationships that could have appeared to influence the work reported in this paper.

Acknowledgments

Appendix A. Supplementary data

Supplementary data to this article can be found online at https://doi.org/10.1016/j.bioactmat.2024.07.034.

References

[1] A. Trounson, C. Mcdonald, Stem cell therapies in clinical trials: progress and challenges, Cell Stem Cell (1) (2015) 11–22.

[2] S.M. Richardson, G. Kalamegam, P.N. Pushparaj, C. Matta, A. Memic, A. Khademhosseini, R. Mobasheri, F.L. Poletti, J.A. Hoyland, A. Mobasheri,

Mesenchymal stem cells in regenerative medicine: focus on articular cartilage and intervertebral disc regeneration, Methods (San Diego, Calif.) (2015) 69–80.

[3] H. Yu, Y. Huang, L. Yang, Research progress in the use of mesenchymal stem cells and their derived exosomes in the treatment of osteoarthritis, Ageing Res. Rev. (2022) 101684.

[4] J. Galipeau, L. Sensébé, Mesenchymal stromal cells: clinical challenges and therapeutic opportunities, Cell Stem Cell (6) (2018) 824–833.

[5] N. Song, M. Scholtemeijer, K. Shah, Mesenchymal stem cell immunomodulation: mechanisms and therapeutic potential, Trends Pharmacol. Sci. (9) (2020) 653–664.

[6] L. Ye, Z. Fan, B. Yu, J. Chang, K.A. Hezaimi, X. Zhou, N. Park, C. Wang, Histone demethylases KDM4B and KDM6B promotes osteogenic differentiation of human MSCs, Cell Stem Cell (1) (2012) 50–61.

[7] S. Golpanian, A. Wolf, K.E. Hatzistergos, J.M. Hare, Rebuilding the damaged heart: mesenchymal stem cells, cell-based therapy, and engineered heart tissue, Physiol. Rev. (3) (2016) 1127–1168.

[8] K. Malekpour, A. Hazrati, S. Soudi, S.M. Hashemi, Mechanisms behind therapeutic potentials of mesenchymal stem cell mitochondria transfer/delivery, J. Contr. Release : Offic. J. Controlled Release Soc. (2023) 755–769.

[9] A. Mokbel, O. El-tookhy, A.A. Shamaa, D. Sabry, L. Rashed, A. Mostafa, Homing and efficacy of intra-articular injection of autologous mesenchymal stem cells in experimental chondral defects in dogs, Clin. Exp. Rheumatol. (2) (2011) 275–284.

[10] S. Jiang, G. Tian, X. Li, Z. Yang, F. Wang, Z. Tian, B. Huang, F. Wei, K. Zha, Z. Sun, X. Sui, S. Liu, W. Guo, Q. Guo, Research progress on stem cell therapies for articular cartilage regeneration, Stem Cell. Int. (2021) 8882505.

[11] Y. Fu, B. Sui, L. Xiang, X. Yan, D. Wu, S. Shi, X. Hu, Emerging understanding of apoptosis in mediating mesenchymal stem cell therapy, Cell Death Dis. 12 (6) (2021) 596.

[12] Z. Li, M. Wu, S. Liu, X. Liu, Y. Huan, Q. Ye, X. Yang, H. Guo, A. Liu, X. Huang, X. Yang, F. Ding, H. Xu, J. Zhou, P. Liu, S. Liu, Y. Jin, K. Xuan, Apoptotic vesicles activate autophagy in recipient cells to induce angiogenesis and dental pulp regeneration, Mol. Ther. : J. Am. Soc. Gene Therapy (2022) 3193–3208.

[13] A. Galleu, Y. Riffo-vasquez, C. Trento, C. Lomas, L. Dolcetti, T.S. Cheung, M. V. Bonin, L. Barbieri, K. Halai, S. Ward, L. Weng, R. Chakraverty, G. Lombardi, F. M. Watt, K. Orchard, D.I. Marks, J. Apperley, M. Bornhauser, H. Walczak, C. Bennett, F. Dazzi, Apoptosis in mesenchymal stromal cells induces in vivo recipient-mediated immunomodulation, Sci. Transl. Med. (416) (2017).

[14] Y. Zhang, S. Liu, W. Guo, M. Wang, C. Hao, S. Gao, X. Zhang, X. Li, M. Chen, X. Jing, Z. Wang, J. Peng, S. Lu, Q. Guo, Human umbilical cord Wharton's jelly mesenchymal stem cells combined with an acellular cartilage extracellular matrix scaffold improve cartilage repair compared with microfracture in a caprine model, Osteoarthritis Cartilage (7) (2018) 954–965.

[15] Y. Zhang, S. Liu, W. Guo, C. Hao, M. Wang, X. Li, X. Zhang, M. Chen, Z. Wang, X. Sui, J. Peng, Y. Wang, S. Lu, Q. Guo, Coculture of hWJMSCs and pACs in oriented scaffold enhances hyaline cartilage regeneration in vitro</i&gt, Stem Cell. Int. (2019) 5130152.

[16] S. Caruso, I.K.H. Poon, Apoptotic cell-derived extracellular vesicles: more than just debris, Front. Immunol. 9 (2018) 1486.

[17] L.R. Grant, I. Milic, A. Devitt, Apoptotic cell-derived extracellular vesicles: structure–function relationships, Biochem. Soc. Trans. 47 (2) (2019) 509–516.

[18] C.B. Medina, P. Mehrotra, S. Arandjelovic, J.S.A. Perry, Y. Guo, S. Morioka, B. Barron, S.F. Walk, B. Ghesquière, A.S. Krupnick, U. Lorenz, K.S. Ravichandran, Metabolites released from apoptotic cells act as tissue messengers, Nature (7801) (2020) 130–135.

[19] S. Caruso, I.K.H. Poon, Apoptotic cell-derived extracellular vesicles: more than just debris, Front. Immunol. (2018) 1486.

[20] H.D. Ryoo, T. Gorenc, H. Steller, Apoptotic cells can induce compensatory cell proliferation through the JNK and the Wingless signaling pathways, Dev. Cell (4) (2004) 491–501.

[21] C. Zheng, B. Sui, X. Zhang, J. Hu, J. Chen, J. Liu, D. Wu, Q. Ye, L. Xiang, X. Qiu, S. Liu, Z. Deng, J. Zhou, S. Liu, S. Shi, Y. Jin, Apoptotic vesicles restore liver macrophage homeostasis to counteract type 2 diabetes, J. Extracell. Vesicles 10 (7) (2021) e12109.

[22] Z. Ding, Z. Yan, X. Yuan, G. Tian, J. Wu, L. Fu, H. Yin, S. He, C. Ning, Y. Zheng, Z. Zhang, X. Sui, L. Hao, Y. Niu, S. Liu, W. Guo, Q. Guo, Apoptotic extracellular vesicles derived from hypoxia-preconditioned mesenchymal stem cells within a modified gelatine hydrogel promote osteochondral regeneration by enhancing stem cell activity and regulating immunity, J. Nanobiotechnol. (1) (2024) 74.

[23] X. Li, S. Li, X. Fu, Y. Wang, Apoptotic extracellular vesicles restore homeostasis of the articular microenvironment for the treatment of rheumatoid arthritis, Bioact. Mater. (2024) 564–576.

[24] C.E. Fogarty, A. Bergmann, Killers creating new life: caspases drive apoptosis-induced proliferation in tissue repair and disease, Cell Death Differ. (8) (2017) 1390–1400.

[25] S. Chera, L. Ghila, K. Dobretz, Y. Wenger, C. Bauer, W. Buzgariu, J. Martinou, B. Galliot, Apoptotic cells provide an unexpected source of Wnt3 signaling to drive hydra head regeneration, Dev. Cell (2) (2009) 279–289.

[26] K.H. Gupta, J.W. Goldufsky, S.J. Wood, N.J. Tardi, G.S. Moorthy, D.Z. Gilbert, J. P. Zayas, E. Hahm, M.M. Altintas, J. Reiser, S.H. Shafikhani, Apoptosis and compensatory proliferation signaling are coupled by CrkI-containing microvesicles, Dev. Cell (6) (2017) 674–684.e5.

[27] C.K. Brock, S.T. Wallin, O.E. Ruiz, K.M. Samms, A. Mandal, E.A. Sumner, G. T. Eisenhoffer, Stem cell proliferation is induced by apoptotic bodies from dying cells during epithelial tissue maintenance, Nat. Commun. (1) (2019) 1044.

[28] S. Jiang, G. Tian, Z. Yang, X. Gao, F. Wang, J. Li, Z. Tian, B. Huang, F. Wei, X. Sang, L. Shao, J. Zhou, Z. Wang, S. Liu, X. Sui, Q. Guo, W. Guo, X. Li, Enhancement of acellular cartilage matrix scaffold by Wharton's jelly mesenchymal stem cell-

derived exosomes to promote osteochondral regeneration, Bioact. Mater. (9) (2021) 2711–2728.

[29] G. Tian, S. Jiang, J. Li, F. Wei, X. Li, Y. Ding, Z. Yang, Z. Sun, K. Zha, F. Wang, B. Huang, L. Peng, Q. Wang, Z. Tian, X. Yang, Z. Wang, Q. Guo, W. Guo, S. Liu, Cell-free decellularized cartilage extracellular matrix scaffolds combined with interleukin 4 promote osteochondral repair through immunomodulatory macrophages: in vitro and in vivo preclinical study, Acta Biomater. 127 (2021) 131–145.

[30] H. Kang, J. Peng, S. Lu, S. Liu, L. Zhang, J. Huang, X. Sui, B. Zhao, A. Wang, W. Xu, Z. Luo, Q. Guo, In vivo cartilage repair using adipose-derived stem cell-loaded decellularized cartilage ECM scaffolds, J. Tissue Eng. Regenerative Med. (6) (2012) 442–453.

[31] D.H. Lee, S.A. Kim, J. Song, A.A. Shetty, B. Kim, S.J. Kim, Cartilage regeneration using human umbilical cord blood derived mesenchymal stem cells: a systematic review and meta-analysis, Medicina (kaunas, Lithuania) 58 (12) (2022) 1801.

[32] J. Song, K. Hong, N. Kim, B. Hwangbo, B. Yang, B.N. Victoroff, N. Choi, Clinical and magnetic resonance imaging outcomes after human cord blood–derived mesenchymal stem cell implantation for chondral defects of the knee, Orthopaedic J. Sports Medicine 11 (4) (2023) 23259671231158391.

[33] J. Wang, L. Zhou, Y. Zhang, L. Huang, Q. Shi, Mesenchymal stem cells - a promising strategy for treating knee osteoarthritis, Bone & Joint Research 9 (10) (2020) 719–728.

[34] T.S.D. Windt, L.A. Vonk, I.C.M. Slaper-Cortenbach, M.P.H.V.D. Broek, R. Nizak, M. H.P.V. Rijen, R.A.D. Weger, W.J.A. Dhert, D.B.F. Saris, Allogeneic mesenchymal stem cells stimulate cartilage regeneration and are safe for single-stage cartilage repair in humans upon mixture with recycled autologous chondrons, Stem Cells (dayton, Ohio) 35 (1) (2016) 256–264.

[35] S. Lee, E. Choi, M. Cha, K. Hwang, Cell adhesion and long-term survival of transplanted mesenchymal stem cells: a prerequisite for cell therapy, Oxid. Med. Cell. Longev. (2015) 632902.

[36] M.B. Preda, C.A. Neculachi, I.M. Fenyo, A. Vacaru, M.A. Publik, M. Simionescu, A. Burlacu, Short lifespan of syngeneic transplanted MSC is a consequence of in vivo apoptosis and immune cell recruitment in mice, Cell Death Dis. (6) (2021) 566.

[37] F. Li, F. Zhang, T. Wang, Z. Xie, H. Luo, W. Dong, J. Zhang, C. Ren, W. Peng, A self-amplifying loop of TP53INP1 and P53 drives oxidative stress-induced apoptosis of bone marrow mesenchymal stem cells, Apoptosis : Inter. J. Programmed Cell Death (5–6) (2024) 882–897.

[38] S. Gulia, P. Chandra, A. Das, The prognosis of cancer depends on the interplay of autophagy, apoptosis, and anoikis within the tumor microenvironment, Cell Biochem. Biophys. (4) (2023) 621–658.

[39] E.A. Guseva, J.A. Pavlova, O.A. Dontsova, P.V. Sergiev, Synthetic activators of autophagy, Biochemistry. Biokhimiia (1) (2024) 27–52.

[40] S. He, H. Deng, P. Li, J. Hu, Y. Yang, Z. Xu, S. Liu, W. Guo, Q. Guo, Arthritic microenvironment-dictated fate decisions for stem cells in cartilage repair, Adv. Sci. 27 (2023) e2207715.

[41] M.S. D'arcy, Cell death: a review of the major forms of apoptosis, necrosis and autophagy, Cell Biol. Int. (6) (2019) 582–592.

[42] E. Boada-romero, J. Martinez, B.L. Heckmann, D.R. Green, The clearance of dead cells by efferocytosis, Nat. Rev. Mol. Cell Biol. (7) (2020) 398–414.

[43] A.C. Doran, A. Yurdagul, I. Tabas, Efferocytosis in health and disease, Nat. Rev. Immunol. (4) (2019) 254–267.

[44] H. Liu, S. Liu, X. Qiu, Y. Yang, L. Bao, F. Pu, X. Liu, C. Li, K. Xuan, J. Zhou, Z. Deng, S. Liu, Y. Jin, Donor MSCs release apoptotic bodies to improve myocardial infarction via autophagy regulation in recipient cells, Autophagy 12 (2020) 2140–2155.

[45] L. Xin, C. Wei, X. Tong, Y. Dai, D. Huang, J. Chen, L. Ma, S. Zhang, In situ delivery of apoptotic bodies derived from mesenchymal stem cells via a hyaluronic acid hydrogel: a therapy for intrauterine adhesions, Bioact. Mater. 12 (2021) 107–119.

[46] C. Zheng, B. Sui, X. Zhang, J. Hu, J. Chen, J. Liu, D. Wu, Q. Ye, L. Xiang, X. Qiu, S. Liu, Z. Deng, J. Zhou, S. Liu, S. Shi, Y. Jin, Apoptotic vesicles restore liver macrophage homeostasis to counteract type 2 diabetes, J. Extracell. Vesicles 10 (7) (2021) e12109.

[47] S. Caruso, I.K.H. Poon, Apoptotic cell-derived extracellular vesicles: more than just debris, Front. Immunol. 9 (2018) 1486.

[48] T. Moldoveanu, Apoptotic mitochondrial poration by a growing list of pore-forming BCL-2 family proteins, Bioessays : News and Reviews in Molecular, Cellular and Developmental Biology 45 (3) (2023) e2200221.

[49] A. Ottosson-Wadlund, R. Ceder, G. Preta, K. Pokrovskaja, R.C. Grafström, M. Heyman, S. Söderhäll, D. Grandér, I. Hedenfalk, J.D. Robertson, B. Fadeel, Requirement of apoptotic protease-activating factor-1 for bortezomib-induced apoptosis but not for fas-mediated apoptosis in human leukemic cells, Mol. Pharmacol. 83 (1) (2012) 245–255.

[50] M. Bakhshoudeh, K. Mehdizadeh, S. Hosseinkhani, F. Ataei, Upregulation of apoptotic protease activating factor-1 expression correlates with anti-tumor effect of taxane drug, Med. Oncol. (northwood, London, England) 38 (8) (2021) 88.

[51] L. Davies, D. Gray, D. Spiller, M.R.H. White, B. Damato, I. Grierson, L. Paraoan, P53 apoptosis mediator PERP: localization, function and caspase activation in uveal melanoma, J. Cell Mol. Med. 13 (8B) (2009) 1995–2007.

[52] L.D. Attardi, E.E. Reczek, C. Cosmas, E.G. Demicco, M.E. Mccurrach, S.W. Lowe, T. Jacks, PERP, an apoptosis-associated target of p53, is a novel member of the PMP-22/gas3 family, Genes Dev. (6) (2000) 704–718.

[53] W. Pei, K. Tanaka, S.C. Huang, L. Xu, B. Liu, J. Sinclair, J. Idol, G.K. Varshney, H. Huang, S. Lin, R.B. Nussenblatt, R. Mori, S.M. Burgess, Extracellular HSP60 triggers tissue regeneration and wound healing by regulating inflammation and cell proliferation, NPJ Regenerative Med. (2016) 16013.

[54] F. Xu, M. Guo, W. Huang, L. Feng, J. Zhu, K. Luo, J. Gao, B. Zheng, L. Kong, T. Pang, X. Wu, Q. Xu, Annexin A5 regulates hepatic macrophage polarization via directly targeting PKM2 and ameliorates NASH, Redox Biol. (2020) 101634.

[55] H. Zhu, G. Wang, H. Zhu, A. Xu, ITGA5 is a prognostic biomarker and correlated with immune infiltration in gastrointestinal tumors, BMC Cancer (1) (2021) 269.

[56] J. Sun, S. Wang, C. Li, Y. Ren, J. Wang, Novel expression profiles of microRNAs suggest that specific miRNAs regulate gene expression for the sexual maturation of female Schistosoma japonicum after pairing, Parasites Vectors 7 (2014) 177.

[57] P.J. Murray, Macrophage polarization, Annu. Rev. Physiol. 79 (2016) 541–566.

[58] L. Qin, J. Yang, X. Su, Y. Lei, L. Dong, H. Chen, C. Chen, C. Zhao, H. Zhang, J. Deng, N. Hu, W. Huang, The miR-21-5p enriched in the apoptotic bodies of M2 macrophage-derived extracellular vesicles alleviates osteoarthritis by changing macrophage phenotype, Genes & diseases (3) (2022) 1114–1129.

[59] Y. Sun, H. Zhang, Y. Zhang, Z. Liu, D. He, W. Xu, S. Li, C. Zhang, Z. Zhang, Li-Mg-Si bioceramics provide a dynamic immuno-modulatory and repair-supportive microenvironment for peripheral nerve regeneration, Bioact. Mater. (2023) 227–242.

[60] N. Zhang, M. Fan, Y. Zhao, X. Hu, Q. Zhu, X. Jiao, Q. Lv, D. Li, Z. Huang, G. Fu, J. Ge, H. Li, W. Zhang, Biomimetic and NOS-responsive nanomotor deeply delivery a combination of MSC-EV and mitochondrial ROS scavenger and promote heart repair and regeneration, Adv. Sci. (2023) e2301440.

[61] S. Alivernini, L. Macdonald, A. Elmesmari, S. Finlay, B. Tolusso, M.R. Gigante, L. Petricca, C.D. Mario, L. Bui, S. Perniola, M. Attar, M. Gessi, A.L. Fedele, S. Chilaka, D. Somma, S.N. Sansom, A. Filer, C. Mcsharry, N.L. Millar, K. Kirschner, A. Nerviani, M.J. Lewis, C. Pitzalis, A.R. Clark, G. Ferraccioli, I. Udalova, C. D. Buckley, E. Gremese, I.B. Mcinnes, T.D. Otto, M. Kurowska-stolarska, Distinct synovial tissue macrophage subsets regulate inflammation and remission in rheumatoid arthritis, Nat. Med. (8) (2020) 1295–1306.

[62] T.L. Fernandes, A.H. Gomoll, C. Lattermann, A.J. Hernandez, D.F. Bueno, M. T. Amano, Macrophage: a potential target on cartilage regeneration, Front. Immunol. (2020) 111.

[63] C. Wu, N.S. Harasymowicz, M.A. Klimak, K.H. Collins, F. Guilak, The role of macrophages in osteoarthritis and cartilage repair, Osteoarthritis Cartilage (5) (2020) 544–554.

[64] S.B. Arya, G. Kumar, H. Kaur, A. Kaur, A. Tuli, ARL11 regulates lipopolysaccharide-stimulated macrophage activation by promoting mitogen-activated protein kinase (MAPK) signaling, J. Biol. Chem. 293 (25) (2018) 9892–9909.

[65] C. Gu, H. Zhang, Y. Gao, Adipose mesenchymal stem cells-secreted extracellular vesicles containing microRNA-192 delays diabetic retinopathy by targeting ITGA1, J. Cell. Physiol. (7) (2020) 5036–5051.

[66] Y. Chen, J. Tong, C. Liu, C. He, J. Xiang, G. Yao, H. Zhang, Z. Xie, MSC-derived small extracellular vesicles mitigate diabetic retinopathy by stabilizing Nrf2 through miR-143-3p-mediated inhibition of neddylation, Free Radic. Biol. Med. (2024) 76–87.

[67] S.U. Islam, J.H. Lee, A. Shehzad, E. Ahn, Y.M. Lee, Y.S. Lee, Decursinol angelate inhibits LPS-induced macrophage polarization through modulation of the NFκB and MAPK signaling pathways, Molecules 23 (8) (2018) 1880.

[68] D. Zhou, C. Huang, Z. Lin, S. Zhan, L. Kong, C. Fang, J. Li, Macrophage polarization and function with emphasis on the evolving roles of coordinated regulation of cellular signaling pathways, Cell. Signal. 26 (2) (2014) 192–197.

[69] X. Mu, W. Shi, Y. Xu, C. Xu, T. Zhao, B. Geng, J. Yang, J. Pan, S. Hu, C. Zhang, J. Zhang, C. Wang, J. Shen, Y. Che, Z. Liu, Y. Lv, H. Wen, Q. You, Tumor-derived lactate induces M2 macrophage polarization via the activation of the ERK/STAT3 signaling pathway in breast cancer, Cell Cycle 17 (4) (2018) 428–438.

[70] C. Zhang, W. Cheng, T. Yang, H. Fang, R. Zhang, Lactate secreted by esophageal cancer cells induces M2 macrophage polarization via the AKT/ERK pathway, Thoracic Cancer (22) (2023) 2139–2148.

[71] Q. Zhang, H. Li, Y. Mao, X. Wang, X. Zhang, X. Yu, J. Tian, Z. Lei, C. Li, Q. Han, L. Suo, Y. Gao, H. Guo, D.M. Irwin, G. Niu, H. Tan, Apoptotic SKOV3 cells stimulate M0 macrophages to differentiate into M2 macrophages and promote the proliferation and migration of ovarian cancer cells by activating the ERK signaling pathway, Int. J. Mol. Med. (1) (2019) 10–22.

[72] H. Hu, W. Liu, C. Sun, Q. Wang, W. Yang, Z. Zhang, Z. Xia, Z. Shao, B. Wang, Endogenous repair and regeneration of injured articular cartilage: a challenging but promising therapeutic strategy, Aging and Disease 12 (3) (2021) 886–901.

[73] Y. Zhang, W. Cheng, B. Han, S. Guo, W. Sei, L. Yu, X. Zhang, Let-7i-5p functions as a putative osteogenic differentiation promoter by targeting CKIP-1, Cytotechnology (1) (2021) 79–90.

[74] Z. Zhang, H. Zhou, F. Sun, J. Han, Y. Han, Circ_FBLN1 promotes the proliferation and osteogenic differentiation of human bone marrow-derived mesenchymal stem cells by regulating let-7i-5p/FZD4 axis and Wnt/β-catenin pathway, J. Bioenerg. Biomembr. (5) (2021) 561–572.

[75] C. Xu, L. Hou, J. Zhao, Y. Wang, F. Jiang, Q. Jiang, Z. Zhu, L. Tian, Exosomal let-7i-5p from three-dimensional cultured human umbilical cord mesenchymal stem cells inhibits fibroblast activation in silicosis through targeting TGFBR1, Ecotoxicol. Environ. Saf. (2022) 113302.

[76] Y. Wang, G. Huang, Z. Wang, H. Qin, B. Mo, C. Wang, Elongation factor-2 kinase acts downstream of p38 MAPK to regulate proliferation, apoptosis and autophagy in human lung fibroblasts, Exp. Cell Res. (2) (2018) 291–298.

[77] P. Ba, X. Duan, G. Fu, S. Lv, P. Yang, Q. Sun, Differential effects of p38 and Erk1/2 on the chondrogenic and osteogenic differentiation of dental pulp stem cells, Mol. Med. Rep. (1) (2017) 63–68.

[78] J. Li, Z. Zhao, J. Liu, N. Huang, D. Long, J. Wang, X. Li, Y. Liu, MEK/ERK and p38 MAPK regulate chondrogenesis of rat bone marrow mesenchymal stem cells through delicate interaction with TGF-beta1/Smads pathway, Cell Prolif. (4) (2010) 333–343.

[79] N. Ma, X. Teng, Q. Zheng, P. Chen, The regulatory mechanism of p38/MAPK in the chondrogenic differentiation from bone marrow mesenchymal stem cells, J. Orthop. Surg. Res. (1) (2019) 434.

[80] S. Glyn-jones, A.J.R. Palmer, R. Agricola, A.J. Price, T.L. Vincent, H. Weinans, A. J. Carr, Osteoarthritis, Lancet (London, England) (9991) (2015) 376–387.

[81] S. Muthu, J.V. Korpershoek, E.J. Novais, G.F. Tawy, A.P. Hollander, I. Martin, Failure of cartilage regeneration: emerging hypotheses and related therapeutic strategies, Nat. Rev. Rheumatol. (7) (2023) 403–416.

[82] Q. Yang, J. Peng, Q. Guo, J. Huang, L. Zhang, J. Yao, F. Yang, S. Wang, W. Xu, A. Wang, S. Lu, A cartilage ECM-derived 3-D porous acellular matrix scaffold for in vivo cartilage tissue engineering with PKH26-labeled chondrogenic bone marrow-derived mesenchymal stem cells, Biomaterials 29 (15) (2008) 2378–2387.

[83] H. Kang, J. Peng, S. Lu, S. Liu, L. Zhang, J. Huang, X. Sui, B. Zhao, A. Wang, W. Xu, Z. Luo, Q. Guo, In vivo cartilage repair using adipose-derived stem cell-loaded decellularized cartilage ECM scaffolds, J. Tissue Eng. Regenerative Med. 8 (6) (2012) 442–453.

[84] Y. Zhang, C. Hao, W. Guo, X. Peng, M. Wang, Z. Yang, X. Li, X. Zhang, M. Chen, X. Sui, J. Peng, S. Lu, S. Liu, Q. Guo, Q. Jiang, Co-culture of hWJMSCs and pACs in double biomimetic ACECM oriented scaffold enhances mechanical properties and accelerates articular cartilage regeneration in a caprine model, Stem Cell Res. Ther. (1) (2020) 180.

[85] S. Jiang, G. Tian, Z. Yang, X. Gao, F. Wang, J. Li, Z. Tian, B. Huang, F. Wei, X. Sang, L. Shao, J. Zhou, Z. Wang, S. Liu, X. Sui, Q. Guo, W. Guo, X. Li, Enhancement of acellular cartilage matrix scaffold by Wharton's jelly mesenchymal stem cell-derived exosomes to promote osteochondral regeneration, Bioact. Mater. 6 (9) (2021) 2711–2728.

[86] Ž. Večerić-haler, A. Cerar, M. Perše, (Mesenchymal) stem cell-based therapy in cisplatin-induced acute kidney injury animal model: risk of immunogenicity and tumorigenicity, Stem Cell. Int. (2017) 7304643.

[87] J.A. Heslop, T.G. Hammond, I. Santeramo, A.T. Piella, I. Hopp, J. Zhou, R. Baty, E. I. Graziano, B.P. Marco, A. Caron, P. Sköld, P.W. Andrews, M.A. Baxter, D.C. Hay, J. Hamdam, M.E. Sharpe, S. Patel, D.R. Jones, J. Reinhardt, E.H.J. Danen, U. Ben-david, G. Stacey, P. Björquist, J. Piner, J. Mills, C. Rowe, G. Pellegrini, S. Sethu, D. J. Antoine, M.J. Cross, P. Murray, D.P. Williams, N.R. Kitteringham, C.E. P. Goldring, B.K. Park, Concise review: workshop review: understanding and assessing the risks of stem cell-based therapies, Stem Cells Translat. Med. (4) (2015) 389–400.